Catalysis Science & Technology

PAPER

View Article Online
View Journal | View Issue

Cite this: *Catal. Sci. Technol.*, 2014, 4, 441

Well-dispersed bimetallic nanoparticles confined in mesoporous metal oxides and their optimized catalytic activity for nitrobenzene hydrogenation

Juanjuan Liu, Shihui Zou, Liping Xiao and Jie Fan*

Received 10th September 2013,
Accepted 20th October 2013

DOI: 10.1039/c3cy00689a

www.rsc.org/catalysis

Well-dispersed bimetallic nanoparticles (BMNPs = PtPd/AuPd/AuPt) confined in mesoporous metal oxides (MMOs = TiO_2/Al_2O_3/SiO_2/ZrO_2) are synthesized by a general and mild one-step sol–gel strategy. This approach allows facile control over the compositional parameter of the supported BMNPs and the MMOs. Moreover, we can also control the formation of the alloy by simply adjusting the loading content. The catalytic results of PtPd–MMO composites in the hydrogenation of nitrobenzene have shown that the performance is highly composition-dependent and support-dependent with Pt_1Pd_3–m-SiO_2 showing the optimum activity.

1. Introduction

Bimetallic nanoparticles (BMNPs) have received considerable attention for their unique catalytic, electrical, magnetic and optical properties, which are very different from those of their monometallic analogues due to synergetic effects between the two elements.[1–6] However, the overall performance of these BMNPs is dependent on the size, shape, crystal structure, and the textural parameters. In order to obtain high catalytic activity, BMNPs are often loaded on support materials[7] or dispersed in liquid phases using polymers/ionic liquids.[8,9] Among the solid supports, mesoporous metal oxides (MMOs) are commonly used. In fact, MMOs could not only protect BMNPs from aggregation and improve their thermal stability, but they could also enhance their catalytic activity by providing surrounding acid/base and redox sites, or desired metal/metal oxide interfaces.[10,11] In this regard, the design and preparation of efficient and stable BMNP–MMO catalysts have been a major direction in many applications especially in the area of catalysis.

At present, various synthetic approaches have been employed to make effective BMNPs–MMOs catalysts. They fall into two major classes: (I) synthesis of BMNPs *via* a successive or simultaneous reduction process, and then loading them on to the MMOs;[10,12–14] (II) impregnating the metallic precursors2 to the preformed MMOs, followed by co-decomposition, co-reduction or other chemical/physical process.[15–19] Despite the fact that various techniques have been utilized to prepare BMNP–MMO, they need complex multi-step procedures for the following reasons. On one hand, the coexistence of bimetallic precursors will complicate the reduction or decomposition kinetics and thus make it more difficult to rationally design the growth process of nanocrystals; on the other hand, the dissimilar growth kinetics and physics/chemistry of the bimetal and metal oxide precursors often lead to undesirable aggregation of BMNPs on the MMOs. Herein we present a general one-step sol–gel strategy for the preparation of BMNP (PtPd/AuPd/AuPt)–MMOs. This approach allows facile control over the compositional parameters of the supported BMNPs as well as the MMOs and alloy formation. Moreover, the uniform BMNPs are highly dispersed throughout the mesoporous MMOs. We also investigate the catalytic performance of bimetallic PtPd–MMOs in the hydrogenation of nitrobenzene and confirm that the performance is highly composition-dependent and support-dependent with Pt_1Pd_3–m-SiO_2 showing the optimum activity.

2. Experimental section

2.1. Synthesis of BMNP–MMO

Typical synthesis of BMNP–MMO (*e.g.* PtPd–m-SiO_2). 10 mmol of TEOS (tetraethoxysilane), 40 mmol of HOAc, 24 mmol of HCl (or HNO_3), 1.6 g F127 ($EO_{96}PO_{70}EO_{96}$, MW = 12 000 g mol^{-1}), and Pt and Pd colloidal nanoparticles† (synthesized according to our previous work)[20] were dissolved in 30 mL of ethanol. The mixture was stirred vigorously for 2 h and transferred into a petri dish (diameter 125 mm). The ethanol was evaporated at 40 °C with a relative humidity 30–80%. After the solvent was evaporated, it was transferred into a 65 °C oven and aged

Key Lab of Applied Chemistry of Zhejiang Province, Department of Chemistry, Zhejiang University, Hangzhou, China. E-mail: jfan@zju.edu.cn; Fax: +86 571 87952338; Tel: +86 571 87952338

† The composition proposed in this manuscript is the total composition not a single nanoparticle composition.

for 24 h. The as-synthesized mesostructured hybrids were calcined at 350 °C in air for 6 h (ramp rate 2 °C min^{-1}) before calcination in a quartz tube furnace using 5% H_2–Ar for 5 h at 550 °C (ramp rate 5 °C min^{-1}) to obtain mesoporous PtPd–SiO_2. ICP-AES was further applied to verify the exact loading amount of Pt/Pd of the PtPd–m-SiO_2 samples. The results showed that a >93% loading efficiency was achieved. Using the same method, we obtained a series of BMNP (PtPd/AuPd/AuPt)–MMO (TiO_2/Al_2O_3/SiO_2/ZrO_2) composites as described in Scheme 1. Compared with our previous work, we focus on the regulation of the alloy, instead of the single metal in this work. And we can also control the alloy formation by adjusting the loading content.

2.2. Synthesis of 1 wt% PtPd–m-SiO_2-Im (impregnation)

Synthesis of m-SiO_2. 10 mmol of TEOS (tetraethoxysilane), 40 mmol of HOAc, 24 mmol of HCl (or HNO_3), and 1.6 g F127 ($EO_{96}PO_{70}EO_{96}$, MW = 12 000 g mol^{-1}) were dissolved in 30 mL of ethanol. The mixture was stirred vigorously for 2 h and transferred into a Petri dish (diameter 125 mm). The ethanol was evaporated at 40 °C with a relative humidity of 30–80%. After the solvent had evaporated, it was transferred into a 65 °C oven and aged for 24 h. The as-synthesized mesostructured hybrids were calcined at 350 °C in air for 6 h (ramp rate 2 °C min^{-1}) to obtain mesoporous m-SiO_2.

Synthesis of 1 wt% Pt_1Pd_3–m-SiO_2-Im. A solution containing m-SiO_2, $PdCl_2$ and $H_2PtCl_6{\cdot}6H_2O$ was stirred for 24 h, and then the mixture was evaporated at 100 °C. The powder was calcined at 350 °C in air for 6 h (ramp rate 2 °C min^{-1}) before being calcined in a quartz tube furnace using 5% H_2–Ar for 5 h at 550 °C (ramp rate 5 °C min^{-1}) to obtain mesoporous PtPd–m-SiO_2-Im.

2.3. Characterization

Wide-angle X-ray diffraction (WAXRD) patterns were recorded on a Rigaku Ultimate IV with Cu Kα radiation. HAADF-STEM images and EDX analyses were recorded on the TECNAI G2 F20 operated at 200 KV. The sample was embedded in epoxy resin, and then microtomed into sub-100 nm ultrathin films at room temperature. These thin film samples floating on water or other solvents were collected by copper mesh with a polymer micro grid for STEM imaging. 12 mg of catalyst was dehydrated in an IR cell for 2 h under vacuum prior to pyridine adsorption. Pyridine was introduced to the IR cell at 150 °C. Pyridine adsorption IR spectra of samples were collected at ambient temperature after adsorption at 150 °C. The small-angle X-ray scattering (SAXS) patterns were collected on a Nanostar U SAXS system (Germany) using Cu Kα radiation at 40 kV and 35 mA to determine structural quality and symmetry. Nitrogen adsorption isotherms were measured at −196 °C on a Micromeritics ASAP 2020 adsorption analyzer. Before the adsorption analysis, calcined samples were outgassed under vacuum at 200 °C in the port of the adsorption analyzer.

2.4. Hydrogenation of nitrobenzene

In a typical catalytic reaction, 50 mg of BMNP–MMO catalyst and 2 mmol nitrobenzene were mixed together in 8.0 ml ethanol, before being placed into a 25 ml flask. Then 4 mmol hydrazine hydrate ($N_2H_4{\cdot}H_2O$) was added into the solution. Immediately after the above mixture was heated at 70 °C under vigorously stirring. The intermediate catalytic products produced at different reaction times were analyzed by GC-MS.

3. Results and discussion

X-Ray diffraction (XRD) measurements of the samples were carried out to determine whether the nanoparticles consisted of a mixture of nanoparticles or an alloy. XRD patterns of Pt_1Pd_3–m-SiO_2 are shown in Fig. 1b. Pt and Pd nanoparticles show peaks that match well with those of fcc Pt (JCPDF 04-0802) and Pd (JCPDF 46-1043). The PtPd nanoparticles show peaks similar to those of the elemental nanoparticles. From the expanded view of the (111) peaks of the three samples,

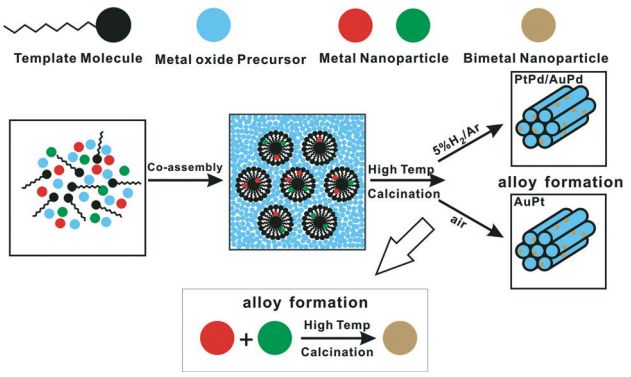

Scheme 1 Schematic of BMNP–MMO synthesis.

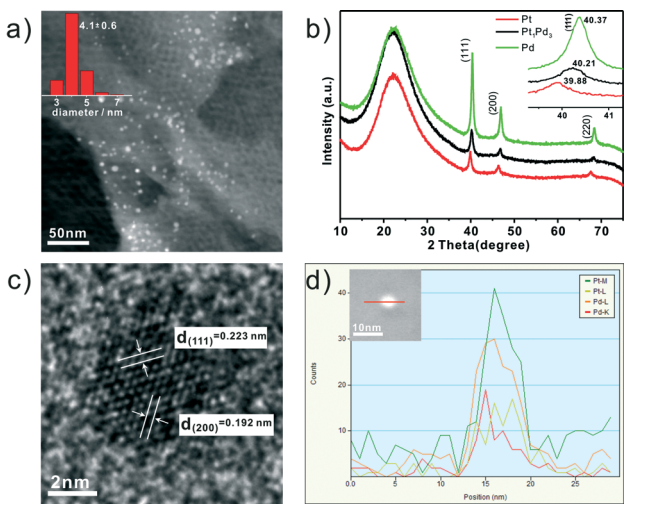

Fig. 1 Characterization of the 1 wt% Pt_1Pd_3–m-SiO_2 sample. a) HAADF-STEM image (particle size distribution inset); b) XRD patterns of Pt, Pd and Pt_1Pd_3–m-SiO_2 (an expanded view of the (111) peaks inset); c) HRTEM image of an individual PtPd NP; d) line-scanning profile across a single PtPdNP (the corresponding bimetallic particle inset).

it can be clearly seen that the position of the (111) peak of Pt_1Pd_3(40.21°) is between that of Pt (39.88°), and Pd (40.37°), indicating the formation of PtPd alloys.[21]

To further confirm the alloy structure, HRTEM and line-scanning analysis were employed. As shown in Fig. 1c, the lattice fringes of Pt_1Pd_3 display interplanar spacings of 0.223 and 0.192 nm in the particle, which match well respectively with those of the (111) and the (200) planes of the fcc PtPd alloy.[22] On the other hand, the compositional line profiles of Pt and Pd cross an individual particle shown in Fig. 1d also suggest the NPs to be alloy with homogeneous distributions of elemental Pt/Pd (note: the size of the electron probe is 1.0 nm, much less than the particle size). Moreover, as can be seen from Fig. 1a, the PtPd NPs are well dispersed in the m-SiO_2 framework and the sizes of PtPd alloy NPs are rather small with a narrow size distribution (4.1 ± 0.6 nm). The mesoporous SiO_2 framework is highly ordered, suggesting that the presence of PtPd NPs does not affect the mesoscopic structure of the oxide support. These results were also confirmed by SAXS data and N_2 adsorption–desorption data. As shown in Fig. 2, the interplanar distance of the (100) plane calculated from the SAXS analysis are both 10 nm. Meanwhile, the results from N_2 adsorption–desorption data confirm that both Pt_1Pd_3–m-SiO_2 and m-SiO_2 have characteristics that are typical of mesoporous materials, and they possess similar BET surface areas (422.8 $m^2\ g^{-1}$ *vs.* 439.4 $m^2\ g^{-1}$), indicating that the introduction of PtPd has little influence on the structure of the MMOs.

The XPS analysis was carried out to study the surface components of PtPd metallic nanoparticles on m-SiO_2. The results in Fig. 3 demonstrate that the binding energy for Pd 3d in the Pt_1Pd_3 alloy has shifted to a lower value compared to that in Pd–m-SiO_2. Whereas the binding energy for Pt 4f in the alloy has shifted to a higher value relative to Pt–m-SiO_2. These shifts demonstrate that some electrons are transferred from Pt to Pd atoms in the alloy structure of PtPd–m-SiO_2, implying that there is a strong electronic interaction between the Pt and Pd in PtPd–m-SiO_2.

The sol–gel approach exhibits excellent advantages in the regulation of the alloy composition. Using this strategy, we can obtain a series of PtPd–m-SiO_2 compounds just by tuning the feed ratio of monometallic PtNPs and PdNPs. From the XRD patterns shown in Fig. 4a, we can see that the (111) peak of PtPd–m-SiO_2 shifts continuously to a higher angle towards the Pd (111) peak as the amount of Pd increases. This is in agreement with the shrinkage of the lattice parameter due to the smaller unit cell parameter of Pd, indicating that the PtPd alloy is formed in all of the PtPd–m-SiO_2 samples.[23–25]

Since the relative amount of each constituent metal in the BMNPs could modify the electronic state of the primary catalytic component and tune the binding properties for intermediate species during the reaction, composition regulation could lead to optimized catalytic performance of BMNPs.[9,26–29] As shown in Fig. 4b, the performance of PtPd–m-SiO_2 in the hydrogenation of nitrobenzene is highly composition-dependent, with Pt_1Pd_3–m-SiO_2 showing the best catalytic activity. Furthermore,

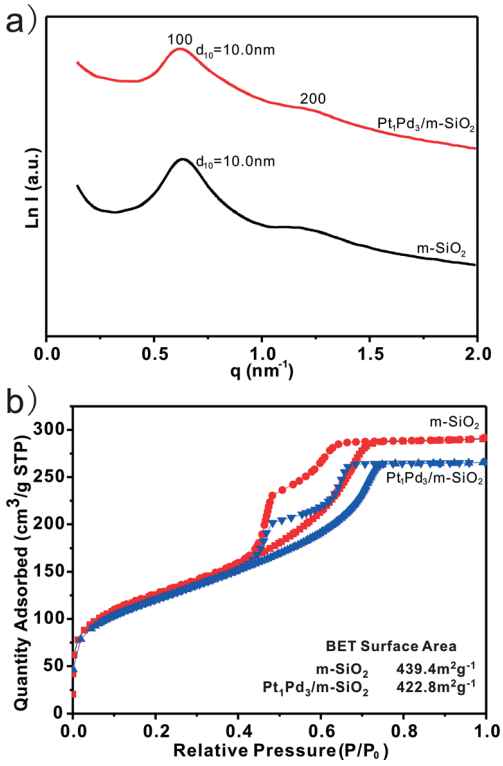

Fig. 2 a) SAXS data for m-SiO_2 and Pt_1Pd_3–m-SiO_2 catalysts; b) N_2 adsorption–desorption isotherms of m-SiO_2 and Pt_1Pd_3–m-SiO_2 catalysts.

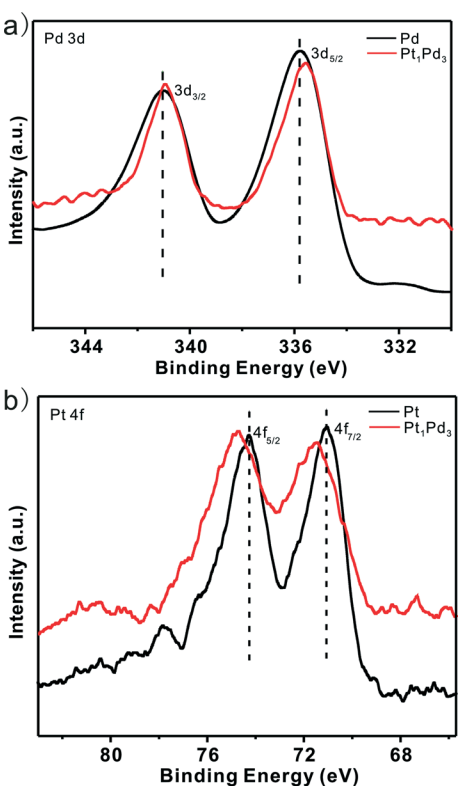

Fig. 3 XPS spectra of Pt and Pd in the 1 wt% Pt_1Pd_3–m-SiO_2 sample (the intensity has been normalized for the comparison).

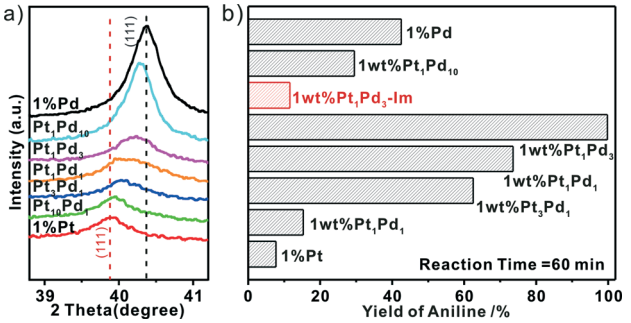

Fig. 4 a) XRD patterns of 1 wt% Pt, Pd, and PtPd–m-SiO_2 catalysts; b) the yields of aniline on 1 wt% Pt–m-SiO_2; PtPd–m-SiO_2; Pd-m-SiO_2 within 60 min (the red bar represents the aniline yield of 1 wt% Pt_1Pd_3 prepared by the impregnation method).

we can see that the hydrogenation reaction on Pt_1Pd_3–m-SiO_2 proceeds very fast. Nearly 90% conversion of nitrobenzene, approaching 100% selectivity to aniline, is achieved within only 10 min, while other compositions show less than 80% yields of aniline even after 60 min reactions. Negligible byproducts (mainly nitrosobenzene) can be detected during the reaction process (Fig. 5). Moreover, the aniline yield of the PtPd–m-SiO_2 is much higher than that of the PtPd catalysts prepared by the conventional impregnation method (99.8% *vs.* 11.6%, within 60 min). There are two major reasons for the greatly enhanced aniline yield of the PtPd–m-SiO_2 compared to that prepared by the conventional impregnation method: 1) the size of the PtPd alloy synthesized by our method (~5 nm) is much smaller the size of the PtPd-Im sample (~21 nm), which offers more surface metal atoms acting as active sites. 2) The highly dispersed PtPd alloy may also increase the catalytic activity, which is confirmed by TEM analysis in our study. It has been reported that the special interaction between PVP, PtNPs, PdNPs and F127 often leads to a high embedding efficiency and good dispersion of the NPs within the MMOs,[30] demonstrating the advantages of our synthetic method.

Besides regulation of the alloy composition, we also tuned the loading concentration of the Pt/Pd nanoparticles. Interestingly, we find there is a critical loading concentration for the formation of PtPd alloys. Combined with their catalytic performance in nitrobenzene hydrogenation, it further confirms that the formation of alloys benefits the reaction. In our case, we believe that the alloy formation is dominated by hetero-atom migration, which only allows a slight growth of the particle size or even a reduction in the size of large nanoparticles.[31,32] The Pt/Pd atoms or clusters are emitted from Pt/Pd particles and migrate to neighboring Pd/Pt particles during the high-temperature calcination process, which is followed by atom rearrangement to form alloy particles. The emission and migration of the Pt/Pd atoms or clusters are confined in mesopores, thus a certain loading amount is required. As can be seen from the XRD patterns in Fig. 6a, the critical loading concentration for the formation of the alloys is 0.4 wt%, and the catalytic performance of 0.4 wt% Pt_1Pd_3 is even better than that of 1 wt% Pd, revealing the superiority of the alloy (Fig. 6b). Once the loading amount is higher than 0.4 wt%, Pt/Pd atoms or clusters can be emitted and transported to neighboring Pd/Pt particles, the nanoparticles mainly exist as the PtPd alloy. In contrast, when the loading amount is as low as 0.2 wt%, the larger distance between neighboring particles does not allow the overlapping of the diffusion spheres of individual nanoparticles. Hetero-atom migration is limited. As a result, the majority of particles exist as Pd nanoparticles with a catalytic performance worse than that of 1 wt% Pd, let alone 0.4 wt% Pt_1Pd_3. The mechanism is similar to the scenario proposed by Tsunehiro Tanaka *et al.*, in which the atom-migrating mechanism was confirmed by *in situ* XAFS and other techniques during the formation of rhodium nanocubes.[33]

The approach is special as it not only regulates the composition of the alloy effectively, but it also facilities the control of the compositional parameter of the oxide supports. When the precursors of MMOs are changed, a variety of metal oxide supports can be obtained,[20] which allow us to evaluate the support effect[25,32,34] of the PtPd alloy for hydrogenation of nitrobenzene. Their yield of aniline within 60 min is 7.8% (m-Al_2O_3), 15.9% (m-ZrO_2), 65.6% (m-TiO_2), 73.6% (m-SiO_2) (Fig. 7). The most active catalyst is obtained with m-SiO_2 while m-Al_2O_3 substantially decreases the activities of the PtPd catalysts, indicating that the added acid sites in alumina supports or the increased metal-support interaction may be unfavorable for the hydrogenation reaction.[35]

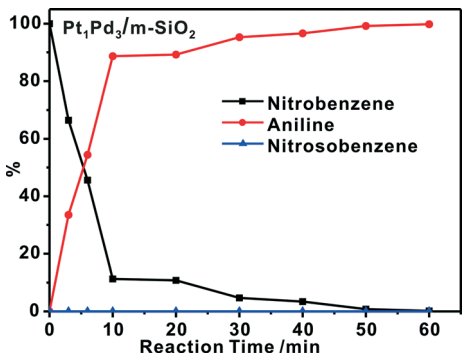

Fig. 5 The time-domain conversion of nitrobenzene and the product selectivity on 1 wt% Pt_1Pd_3–m-SiO_2.

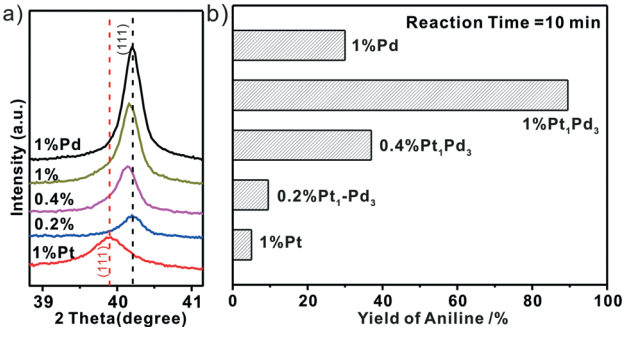

Fig. 6 a) XRD patterns of 1 wt% Pt, 1 wt% Pd, and Pt_1Pd_3–m-SiO_2 catalysts; b) the yields of aniline on 1 wt% Pt–m-SiO_2; 1 wt% Pd–m-SiO_2 ; Pt_1Pd_3–m-SiO_2 within 10 min.

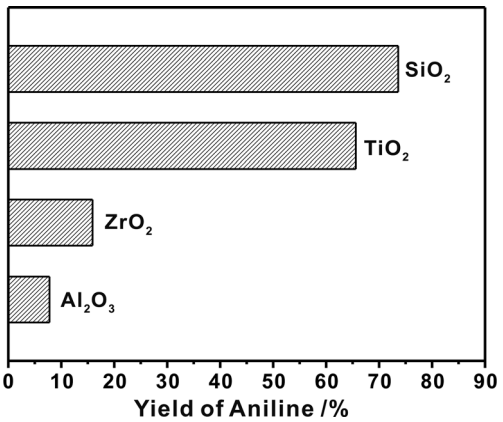

Fig. 7 The yields of aniline on the 1 wt% Pt_1Pd_1–MMOs (M = Al, Zr, Ti and Si) samples within 60 min.

Apart from this, we can also synthesize composite metal oxide supports by introducing another homogeneously distributed component, which may promote improved catalytic performance. The introduction of a small amount of Ti (5%) into the m-SiO_2 framework promotes the activity of the Pt_1Pd_1–m-SiO_2, with the yield of aniline increasing from 73.6% to 86.7% within 60 min (see Fig. 8a). The increased activity may relate to the increase acidity effect, and the acidic properties are also verified by pyridine adsorption IR spectra (see Fig. 8b). Compared to the 1% Pt_1Pd_1–SiO_2 sample, the 1% Pt_1Pd_1/5% TiO_2–SiO_2 sample showed an increased pyridine adsorption peak at 1446 cm^{-1}, which is attributed to the Lewis acid sites.

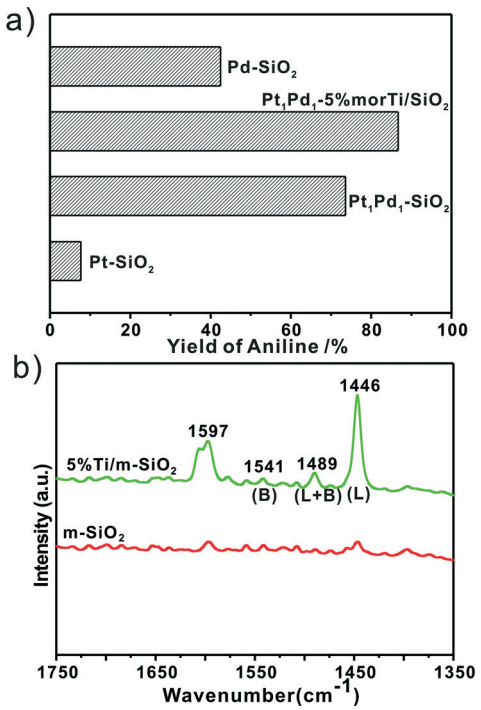

Fig. 8 a) The yields of aniline on the 1% Pt_1Pd_1 catalysts within 60 min; b) FTIR spectra of adsorbed pyridine on m-SiO_2 and 5% Ti–m-SiO_2 at 150 °C.

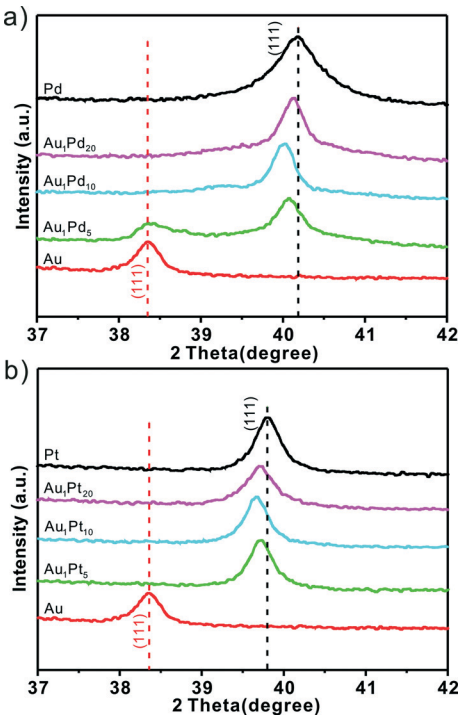

Fig. 9 a) XRD patterns of Au, Pd, and AuPd–m-SiO_2 catalysts; b) XRD patterns of Au, Pt and AuPt–m-SiO_2 catalysts.

Using the same method, we can also synthesize AuPt alloys and AuPd alloys supported on the MMOs (Fig. 9). A variety of BMNP (PtPd/AuPd/AuPt)–MMOs (TiO_2/Al_2O_3/SiO_2/ZrO_2) can be prepared by introducing different MNPs and metal oxide precursors in this way—revealing the proposed process is a general method.

4. Conclusions

In summary, we have developed a general one-step sol–gel process to synthesize BMNP (PtPd/AuPd/AuPt)–MMOs (TiO_2/Al_2O_3/SiO_2/ZrO_2) *via* an assembly process and a high temperature calcination process. This approach allows not only facile control over the compositional parameter of the supported BMNPs but also the oxide support MMOs and we can also control the alloy formation by adjusting the loading content. The catalytic activities of the PtPd–m-SiO_2 in the hydrogenation of nitrobenzene indicate that the performance is highly composition-dependent and support-dependent with Pt_1Pd_3–m-SiO_2 showing the best catalytic activity.

Acknowledgements

This work was supported by the National Science Foundation of China (21222307 and 21003106), Fok Ying Tung Education Foundation (131015), Zhejiang Provincial Natural Science Foundation of China (R12B030002), and the Fundamental Research Funds for the Central Universities (2012QNA3014).

Notes and references

1 S. I. Sanchez, M. W. Small, J. M. Zuo and R. G. Nuzzo, *J. Am. Chem. Soc.*, 2009, **131**, 8683–8689.
2 T. Wu, D. J. Childers, C. Gomez, A. M. Karim, N. M. Schweitzer, A. J. Kropf, H. Wang, T. B. Bolin, Y. Hu, L. Kovarik, R. J. Meyer and J. T. Miller, *ACS Catal.*, 2012, **2**, 2433–2443.
3 X. Yang, Q. D. Yang, J. Xu and C. S. Lee, *J. Mater. Chem.*, 2012, **22**, 8057–8062.
4 B. Pawelec, V. La Parola, R. M. Navarro, S. Murcia-Mascarós and J. L. G. Fierro, *Carbon*, 2006, **44**, 84–98.
5 A. Cao and G. Veser, *Nat. Mater.*, 2010, **9**, 75–81.
6 R. T. Mu, Q. A. Fu, H. Xu, H. I. Zhang, Y. Y. Huang, Z. Jiang, S. O. Zhang, D. L. Tan and X. H. Bao, *J. Am. Chem. Soc.*, 2011, **133**, 1978–1986.
7 Z. Yin, M. Chi, Q. Zhu, D. Ma, J. Sun and X. Bao, *J. Mater. Chem. A*, 2013, **1**, 9157–9163.
8 K. Akamatsu, T. Kawamura, H. Nabika, S. Deki, T. Strunskus and F. Faupel, *J. Mater. Chem.*, 2002, **12**, 3610–3614.
9 X. Yuan, G. Sun, H. Asakura, T. Tanaka, X. Chen, Y. Yuan, G. Laurenczy, Y. Kou, P. J. Dyson and N. Yan, *Chem.–Eur. J.*, 2013, **19**, 1227–1234.
10 H.-L. Jiang, T. Akita, T. Ishida, M. Haruta and Q. Xu, *J. Am. Chem. Soc.*, 2011, **133**, 1304–1306.
11 Y. Chen, H. Wang, C.-J. Liu, Z. Zeng, H. Zhang, C. Zhou, X. Jia and Y. Yang, *J. Catal.*, 2012, **289**, 105–117.
12 L. Liu, G. Samjeske, S. Nagamatsu, O. Sekizawa, K. Nagasawa, S. Takao, Y. Imaizumi, T. Yamamoto, T. Uruga and Y. Iwasawa, *J. Phys. Chem. C*, 2012, **116**, 23453–23464.
13 F. Chassagneux, L. Bois, J.-P. Simon, C. Desroches and A. Brioude, *J. Mater. Chem.*, 2011, **21**, 11947–11955.
14 K.-Y. Chan, J. Ding, J. Ren, S. Cheng and K. Y. Tsang, *J. Mater. Chem.*, 2004, **14**, 505–516.
15 A. Ungureanu, B. Dragoi, A. Chirieac, S. Royer, D. Duprez and E. Dumitriu, *J. Mater. Chem.*, 2011, **21**, 12529–12541.
16 D. Xiang and L. Yin, *J. Mater. Chem.*, 2012, **22**, 9584–9593.
17 T. Garcia, R. Murillo, S. Agouram, A. Dejoz, M. J. Lazaro, L. Torrente-Murciano and B. Solsona, *Chem. Commun.*, 2012, **48**, 5316–5318.
18 B. Folch, J. Larionova, Y. Guari, L. Datas and C. Guerin, *J. Mater. Chem.*, 2006, **16**, 4435–4442.
19 P. L. Dhepe, A. Fukuoka and M. Ichikawa, *Chem. Commun.*, 2003, 590–591.
20 J. Liu, S. Zou, S. Li, X. Liao, Y. Hong, L. Xiao and J. Fan, *J. Mater. Chem. A*, 2013, **1**, 4038–4047.
21 S. Alayoglu and B. Eichhorn, *J. Am. Chem. Soc.*, 2008, **130**, 17479–17486.
22 X. Q. Huang, Y. J. Li, H. L. Zhou, X. F. Duan and Y. Huang, *Nano Lett.*, 2012, **12**, 4265–4270.
23 K. Kusada, M. Yamauchi, H. Kobayashi, H. Kitagawa and Y. Kubota, *J. Am. Chem. Soc.*, 2010, **132**, 15896–15898.
24 X. Yang, Q. Yang, J. Xu and C.-S. Lee, *J. Mater. Chem.*, 2012, **22**, 8057–8062.
25 L. Li, Z. Niu, S. Cai, Y. Zhi, H. Li, H. Rong, L. Liu, L. Liu, W. He and Y. Li, *Chem. Commun.*, 2013, **49**, 6843–6845.
26 S. Zhang, O. Metin, D. Su and S. H. Sun, *Angew. Chem., Int. Ed.*, 2013, **52**, 3681–3684.
27 F. Tao, M. E. Grass, Y. W. Zhang, D. R. Butcher, F. Aksoy, S. Aloni, V. Altoe, S. Alayoglu, J. R. Renzas, C. K. Tsung, Z. W. Zhu, Z. Liu, M. Salmeron and G. A. Somorjai, *J. Am. Chem. Soc.*, 2010, **132**, 8697–8703.
28 H. C. Ye and R. M. Crooks, *J. Am. Chem. Soc.*, 2007, **129**, 3627–3633.
29 H. Zhang, Y. J. Yin, Y. J. Hu, C. Y. Li, P. Wu, S. H. Wei and C. X. Cai, *J. Phys. Chem. C*, 2010, **114**, 11861–11867.
30 H. Song, R. M. Rioux, J. D. Hoefelmeyer, R. Komor, K. Niesz, M. Grass, P. Yang and G. A. Somorjai, *J. Am. Chem. Soc.*, 2006, **128**, 3027–3037.
31 X. Peng, *Nano Res.*, 2009, **2**, 425–447.
32 X. Yan, X. Wang, Y. Tang, G. Ma, S. Zou, R. Li, X. Peng, S. Dai and J. Fan, *Chem. Mater.*, 2013, **25**, 1556–1563.
33 S. Yao, Y. Yuan, C. Xiao, W. Li, Y. Kou, P. J. Dyson, N. Yan, H. Asakura, K. Teramura and T. Tanaka, *J. Phys. Chem. C*, 2012, **116**, 15076–15086.
34 W. G. Menezes, V. Zielasek, K. Thiel, A. Hartwig and M. Bäumer, *J. Catal.*, 2013, **299**, 222–231.
35 G. C. Bond, C. Louis and D. T. Thompson, *Catalysis by Gold*, Imperial College Press, 2006.

